ELSEVIER

Journal of Nuclear Materials 252 (1998) 34–42

journal of nuclear materials

A temperature threshold for gas–bubble superlattice formation in molybdenum

F.E. Lawson *, P.B. Johnson

School of Chemical and Physical Sciences, Victoria University of Wellington, PO Box 600, Wellington, New Zealand

Received 1 April 1997; accepted 3 October 1997

Abstract

He irradiation of metals at temperatures around $0.2T_m$ (T_m is the melting point of the metal) commonly results in the formation of small (≈ 2 nm) bubbles in high concentration ($\approx 10^{25}$ m^{-3}) ordered on a superlattice. Previous work has established that there is an upper temperature limit for bubble ordering of $\approx 0.35T_m$. Here we report the results of the first comprehensive investigation of the possible existence of a lower temperature limit. Mo is implanted with He at temperatures in the range $0.07T_m$ to $0.20T_m$. For the implantations above $0.16T_m$, TEM studies show that the bubbles are ordered on a superlattice. In contrast at lower implantation temperatures only random bubble arrays are found. It is demonstrated that there is a lower temperature threshold for bubble ordering in Mo in the temperature range $0.14T_m$ to $0.16T_m$. This range correlates well with the 'onset' temperature for thermally stimulated vacancy motion in Mo. © 1998 Elsevier Science B.V.

1. Introduction

Transmission electron microscope (TEM) studies have revealed ordered bubble arrays in a variety of metals that have undergone ion-implantation of inert gases. Early studies demonstrated bubble superlattice formation in the bcc metal molybdenum [1,2] and the fcc metals copper, nickel and stainless steel [3–6]. Bubble ordering was also found in the hcp metal titanium [5,7–9], but the ordering was not as fully developed as in the other two classes of metals. Bubble ordering has been the subject of regular review articles, for example [10–12]. The most recent research is reported in Refs. [13–15]. Bubble ordering takes the form of either (i) bubbles ordered onto regularly spaced planes, but not within those planes, or (ii) full three-dimensional ordering where the bubbles form a superlattice.

A recent study of bcc metals has found that for implantation temperatures around $0.2T_m$ bubble superlattices were formed in all six metals investigated [13]. These observations taken together with the earlier research reviewed in Ref. [12], strongly suggest that bubble ordering is a universal phenomenon for implantation temperatures around $0.2T_m$, irrespective of the metal crystal type.

The foundation studies of bubble ordering in molybdenum by Sass and Eyre [1] and by Mazey et al. [2] reported superlattice formation for helium implantation over a wide range of temperatures including temperatures below 400 K ($0.14T_m$). For many years it was widely assumed that there was no lower temperature limit for superlattice formation and that bubble ordering would occur however low the implantation temperature. These studies established a higher temperature limit for bubble superlattice formation of approximately $0.35T_m$.

In 1986, Johnson and Mazey carried out a new study of bubble ordering in molybdenum in an attempt to resolve some inconsistencies in earlier work. They could find no evidence of bubble ordering at temperatures below 400 K even though several different helium current densities and dose levels were used. They found the results somewhat confusing and so reporting them was delayed until the 1995 study [13]. These authors pointed out that the earlier experiments [1,2] had involved implantation into pre-

* Corresponding author. Present address: Measurement Standards Laboratory of New Zealand, Industrial Research Ltd., PO Box 31-310, Lower Hutt, New Zealand. Fax: +64-4 566 6004.

PII S0022-3115(97)00298-5

thinned specimens and may not have excluded heating of the target by the ion-beam. In such a case the actual temperature, especially in the thinnest regions of the specimen, could be in excess of that indicated by a thermocouple attached to the bulk part of the target or the target holder. It was observed that the 1986 results, although too fragmentary to draw firm conclusions, were consistent with the existence of a lower implantation temperature threshold for helium bubble ordering in molybdenum.

Implantation into pre-thinned foils, rather than into bulk foils (which are thinned after implantation for EM examination), introduces some additional uncertainties. For example, in a pre-thinned foil the second surface close to the implanted layer could facilitate ordering by acting as a second source of vacancies and as a sink for defects such as dislocations. Also, in very thin samples, there is the possibility that some of the helium ions may pass through and not be stopped in the foil, making accurate statements about the dose level difficult. For the above reasons bulk foils are used here.

The present work is the first comprehensive study specifically aimed at determining the existence (or otherwise) of a lower temperature threshold for bubble ordering in a helium implanted metal. Amongst the metals studied previously, the best example of bubble ordering (i.e. the bubble lattice with the highest degree of lattice perfection) was found in the bcc metal molybdenum [2]. In one case [13] the degree of lattice perfection was sufficient to give rise to second order, as well as first order reflections from bubble planes. It was this tendency to form highly ordered bubble structures that led to molybdenum being chosen for the present study.

Establishing the existence of a lower temperature threshold could provide valuable insights into the mechanisms responsible for bubble ordering and the development of radiation damage structures more generally.

2. Experimental

Molybdenum foils of thickness 0.050 mm and purity 99.9% were annealed in vacuum to produce grains of a suitable size for analysis. After mechanical polishing, the foils were implanted with helium in a modified PN400 Van de Graaff accelerator. The ion energy was 160 keV, with the beam directed at 60° to the surface normal. The distribution of helium with depth is a bell-shaped curve, with the maximum concentration of helium occurring at a depth d_0, corresponding to R_p, the mean projected range for the incident ions. Here d_0 is calculated (using TRIM 95 [16]) to be 225 nm. Similarly the damage, in the form of interstitial–vacancy pairs, is a bell-shaped curve centred on a depth that is somewhat less than d_0.

Implantations were to the critical dose for radiation blistering of the target surface (ϕ_c), and to selected fractions of ϕ_c. In preliminary experiments it was found that ϕ_c depended on the target temperature, ranging from 10^{23} He^+ m^{-2} at 220 K to 6×10^{22} He^+ m^{-2} at 570 K. From previous research gas bubble lattices are known to form in molybdenum for implantation temperatures (T) of $0.2T_m$, and above. Here, values of T between 190 K ($0.07T_m$) and 570 K ($0.20T_m$) were chosen to give a broad range of temperatures below $0.2T_m$.

After irradiation, 3 mm discs were punched from the foil and electrochemically polished from the rear in a Struers' Tenupol 3, using a solution of 14% sulphuric acid and 86% ethanol. A small hole is produced, the edges of which are thin enough to be electron transparent. This polishing regime, which was developed using 3 mm discs punched from unimplanted molybdenum, resulted in good, electron-transparent regions. However, when the solution was used on discs taken from implanted foils, it was found that the electron transparency was poor. For implanted discs, after the chemical back-thinning, further thinning from the back surface using ion-beam milling was required to obtain good quality specimens. The thinned sections were typically 40 to 80 nm in thickness and encompassed a depth region that included the implanted surface. Such specimens, which in terms of depth correspond to the first 60 nm of the implanted layer, are referred to as near-surface specimens.

To investigate bubble structures at greater depths in the target, specimens corresponding to different depths were prepared using a depth profiling technique based on removing controlled amounts of metal from the implanted surface by ion-beam milling [12,14].

Specimens were examined using TEM in a Philips EM 420ST 120 keV electron microscope, operating at a voltage of 100 keV. Images of the bubbles were recorded at high magnification (×135k) in both under- and over-focus conditions. Selected area diffraction patterns (SADPs) were taken from both ordered and random bubble arrays with the electron beam directed close to a principal zone axis of the metal. A high degree of bubble ordering can give rise to extra reflections in the electron diffraction pattern. These reflections appear as satellite spots around the matrix reflections. In the text and figures, we will use a subscript convention to distinguish between reflections from the metal and from the bubble lattice: a subscript 'b' denotes a reflection from the bubble lattice. Where the bubble lattice is parallel with the host lattice, the satellite spots are oriented in the same direction as the low-order matrix reflections. This provides a basis for indexing the satellite reflections. The dominant reflections from the bubble array are those from the dense-packed bubble planes which for a bcc lattice are the $\{110\}_b$ planes.

In the case of ordered bubbles, bubble plane spacings were deduced from the separation of superlattice reflections in the SADP. For random arrays the diameter of a Debye–Scherrer ring in diffraction patterns allowed an estimate to be made of the preferred inter-bubble separation. For both ordered and random arrays, the inter-bubble

Table 1
Sample data

T_i (K)	T_i/T_m	Dose ($\times 10^{22}$ He^+ m^{-2})	ϕ/ϕ_c (%)	Comments on bubble structure
570	0.20	6.3	100	strongly ordered in 3-d
570	0.20	4.7	75	weakly ordered in 3-d
570	0.20	5.5	100	strongly ordered in 3-d
550	0.19	7.4	100	ordered in 3-d
510	0.18	11.4	100	ordered in 3-d
470	0.16	13.6	100	ordered in 3-d
420	0.14	5.4	76	randomly distributed bubbles
390	0.13	10.9	100	randomly distributed bubbles
390	0.13	14.5	74	randomly distributed bubbles
290	0.10	19.4	155	randomly distributed bubbles
290	0.10	12.8	100	randomly distributed bubbles
290	0.10	5.4	42	no bubble structure found
220	0.08	15.2	100	randomly distributed bubbles
220	0.08	11.5	76	randomly distributed bubbles
220	0.08	5.4	36	no bubble structure found

spacings found from diffraction were checked against spacings measured from bright-field micrographs.

3. Results

A large number of specimens was examined representing different implantation temperatures, helium doses and depths below the implanted surface. The results are presented in detail below. Also, to provide an overview, data for some representative near-surface specimens are summarised in Table 1. The implantation temperature, helium dose and observed bubble structure are listed for each specimen.

3.1. Ordered bubbles

As expected, ordered bubbles were found in near-surface specimens taken from targets implanted to ϕ_c at 570 K. A typical example, taken with the beam directed close to [001], is shown in Fig. 1. Satellite reflections from

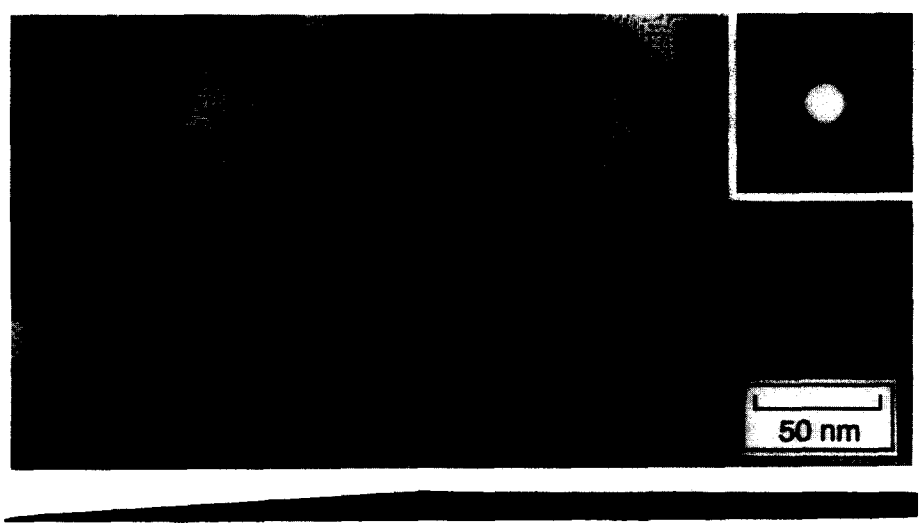

Fig. 1. An electron micrograph (over-focus contrast) of helium bubbles in molybdenum following implantation to ϕ_c (6.3×10^{22} He^+ m^{-2}) at 570 K. The electron beam direction is close to ⟨001⟩. The 110 trace directions are at right angles and parallel to the sides of the figure; bubble rows are evident in these directions. The inset is a section of the corresponding electron diffraction pattern showing two sets of satellites around the 000 transmitted beam. These spots lie in the directions of the matrix 110 spots, and give a bubble lattice constant of 5.1 ± 0.3 nm.

the bubble lattice can be seen around both the transmitted 000 spot and the matrix spots. 110_b reflections are present around 000, and their radial separation gives a lattice constant of 5.1 ± 0.3 nm. However, the satellite reflections around 110 are directed towards the 200 reflections. Their spacing and directions are such that they must be indexed as 100_b reflections, to be consistent with the lattice parameter above. For a bcc lattice, 100 reflections are normally disallowed; the significance of this result is discussed in Section 4.2.

Ordering was also found in near-surface specimens from a target implanted at 570 K to a helium dose level of $0.75\phi_c$. The ordering was found to be weaker than for the specimens implanted to the critical dose. Not only were the satellites from the dense-packed planes weaker than in the ϕ_c case, but they were often radially elongated. This type of elongation indicates the presence in the ordered array of a wide range of {110} interplanar bubble spacings. Also present in the diffraction patterns were disallowed reflections from bubble planes of lower bubble density – bubble planes that are defined by the intersection of the dense-packed {110} bubble planes.

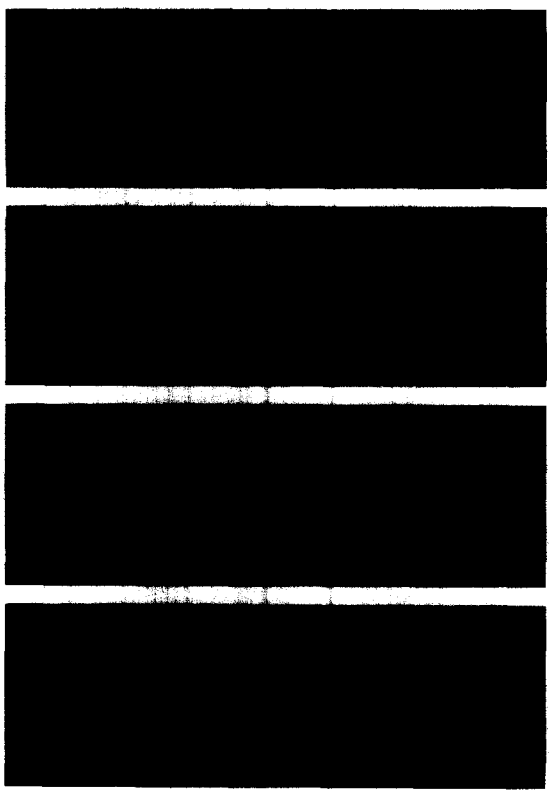

Fig. 2. Sections of electron diffraction patterns taken from helium implanted molybdenum specimens following implantation at temperatures of (a) 570 K, (b) 510 K, (c) 470 K, and (d) 390 K. The electron beam direction is close to ⟨100⟩ in (a), (b) and (c), and ⟨111⟩ in (d). In (a), (b) and (c), the satellites evident around the 000 transmitted beam show that bubbles are ordered. In (d) satellites are not present, indicating that the bubbles are randomly arranged. In each of (b) and (c), satellite spots around the 011 matrix spots (which have not survived reproduction here) were assigned {100} type indices (indices which are disallowed under normal bcc selection rules, see Section 4.2).

The results obtained here are consistent with the following interpretation. There are domains in the bubble structure; within any given domain the bubbles are all of similar size and are relatively well-ordered in three dimensions, with a well-defined lattice constant a_l. However, the average bubble size varies widely from one domain to another and these differences in bubble size result in differences in bubble separation (and hence in a_l) between domains. Since there are many domains lying within the diffraction aperture, this gives rise to radial elongation of the satellite reflections.

Lower implantation temperatures were then investigated. Implantation to ϕ_c was carried out at temperatures of 510 K, 470 K and 390 K. Fig. 2 shows diffraction patterns from bubble arrays in specimens implanted at 570 K and the three lower temperatures. As the implantation temperature was decreased, the satellite reflections in the diffraction pattern became progressively weaker. At the lowest temperature of 390 K, satellites could not be detected and only the bright halo around the transmitted beam remained. This initial evidence suggests that for implantation temperatures above 470 K, ordered bubble lattices are produced, but at temperatures of and below 390 K only randomly oriented bubbles are found.

3.2. Randomly arranged bubbles

Implantation to ϕ_c at temperatures of 390 K and below produced a bubble array that was random in the near-surface region of the sample. Fig. 3 shows a bubble array in a sample implanted at room temperature, with **B** near [001]. Even though there are random bubbles near the surface, it is still possible that in a sample such as this there is bubble ordering occurring below the surface where the helium concentration is greater. To check this possibility, specimens were prepared from different points on the helium concentration profile (i.e. from different depths). This was done using ion-beam milling (IBM) from the front surface to depth profile the sample. It should be noted that specimens from different depths in the same target correspond to different helium to damage ratios as well as to different helium concentrations.

3.3. Depth profiling

To investigate the bubble structure at depths below the surface, a target implanted to ϕ_c at 390 K was depth profiled. After each IBM stage, the specimen was examined in the TEM and the bubble images photographed. Typical images taken from a specimen corresponding to a

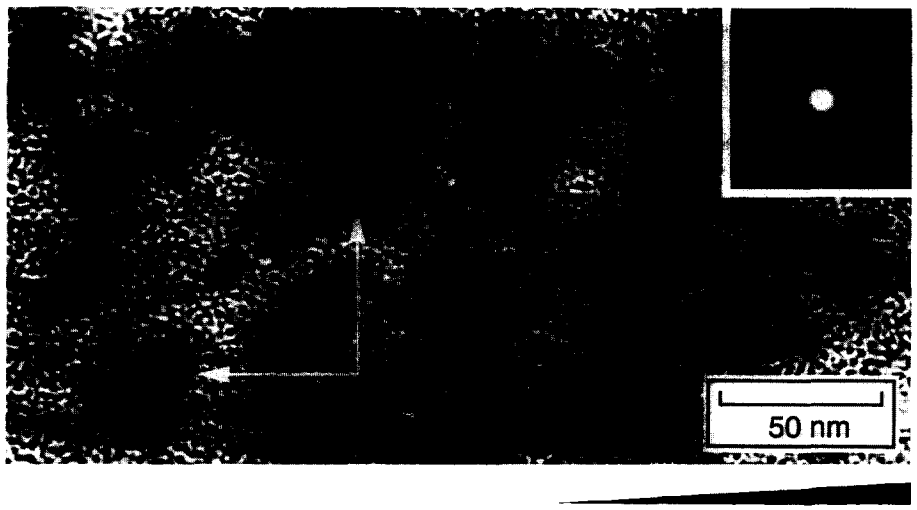

Fig. 3. An electron micrograph (over-focus contrast) of helium bubbles in molybdenum following implantation to $1.6\phi_c$ (1.9×10^{23} He^+ m^{-2}) at 290 K. The electron beam is close to $\langle 001 \rangle$, and trace directions of the $\{110\}$ planes normal to the surface are shown, although there is no bubble alignment evident in these directions. The corresponding electron diffraction pattern does not contain any satellite spots; the bright disc indicates randomly oriented bubbles with a range of inter-bubble spacings.

depth intermediate between the surface and d_0 are shown in Fig. 4. With further IBM, the bubble structure is coarser. The average bubble diameter increases from 1.08 ± 0.04 nm for near-surface specimens, to 1.42 ± 0.04 nm after 30 min IBM. After 50 min IBM, a new type of bubble structure comprising larger bubbles has appeared, being far more porous than the bubble structure at the surface. The largest cavities are found in specimens front milled for 70 min. Here, 'layers' of large, random, irregularly sized bubbles are found. The plane of any given layer is parallel with the specimen surface; the different layers correspond to different depths below the surface. The apparent inter-

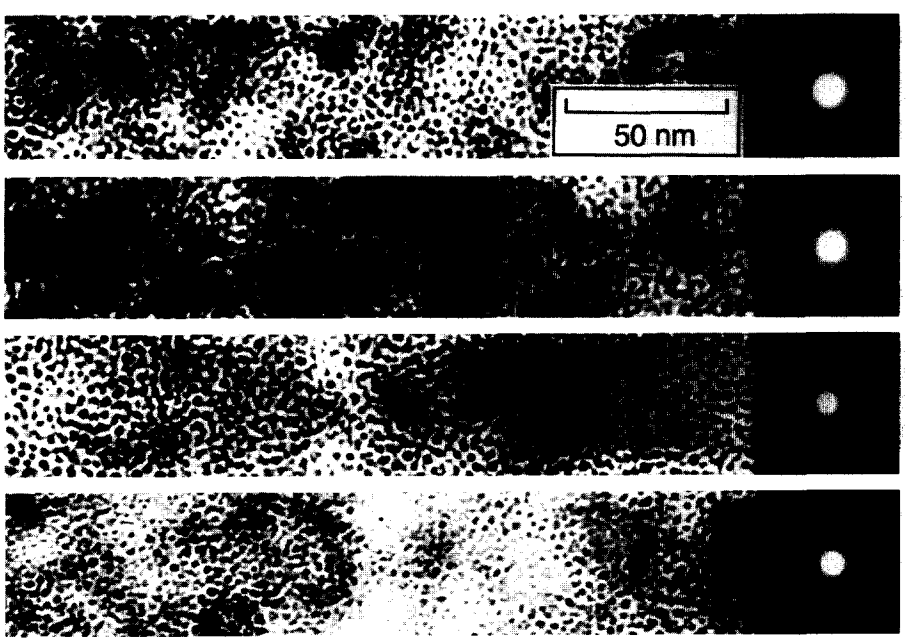

Fig. 4. Bright field micrographs taken after various periods of ion-beam milling (IBM) of the front surface of a sample implanted to ϕ_c at 390 K. The aim is to determine whether bubble ordering has taken place at depths in the sample where the helium concentration is greater than at the surface. The specimen is shown after total IBM times of (a) 10 min, (b) 20 min, (c) 50 min, and (d) 70 min. A general coarsening of the bubble structure is found as the depth increases, but there is no indication of bubble ordering.

connection of cavities found in these specimens is even more pronounced than that found in the 50 min specimens. After 90 min IBM the structure is very similar to that observed in the early stages of IBM. These results suggest that 70 min IBM corresponds approximately to the depth d_0.

Where specimens containing *ordered* bubbles had been subjected to IBM, a similar increase in the average bubble diameter was noted, as well as a small increase in the bubble lattice constant. Ordering was maintained, but at depths near R_p, bright Debye–Scherrer rings were evident in diffraction in addition to the satellite spots. This effect has been seen in earlier IBM experiments [17] and indicates that at depths where there is a high helium concentration, the degree of ordering weakens, but the bubbles maintain a preferred spacing.

3.4. Constant dose experiments

Of particular interest was the effect of dose on bubble formation as it has been suggested that bubble growth depends more on local helium concentration than on local damage [14]. One set of experiments involved implanting targets to the same helium dose (5.4×10^{22} He^+ m^{-2}) at different temperatures and examining the bubble structures in near-surface specimens. At 570 K, radiation blistering was observed on the target surface, and in TEM examination of near-surface specimens, ordered bubble structures (typical bubble diameter 1 nm) were found. At the lower temperatures (420 K, 290 K, 220 K) there was no evidence of blistering of the target surface, and bubbles were found only in the 420 K specimen. These bubbles, which were random, had diameters between 0.6 and 0.8 nm. Because of the relatively small size of these bubbles, we shall take 390 K, rather than 420 K, to be the highest temperature at which only randomly arrayed bubbles were observed. Further discussion about lattice development will be found in Section 4.1.

All four targets had the same local helium and damage concentrations, yet bubble development was far more advanced in the higher temperature cases. This strongly suggests that defect mobility is an important factor in bubble development; at low temperatures this mobility is low and bubble development is restricted. This is discussed further in Section 4.3.

3.5. Bubble parameters

Bubble diameter and spacing were measured for a variety of samples containing both ordered and random bubbles. Fig. 5 shows bubble diameter distributions for random and ordered bubble arrays at the critical dose. Each data set is approximately normally distributed. The difference in the means of the two distributions is less than the experimental uncertainty in determining the bubble diameter.

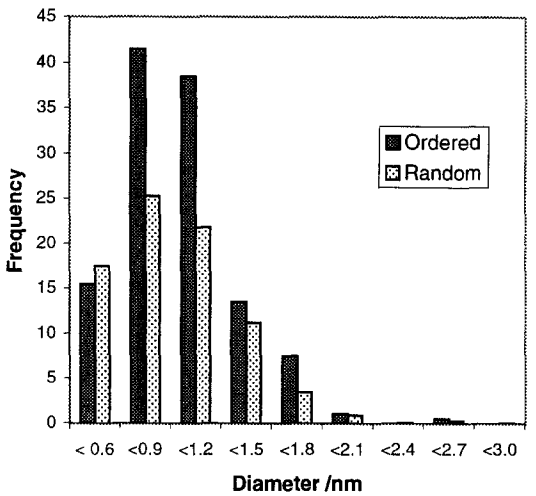

Fig. 5. Histograms of bubble diameter for both ordered and randomly arrayed bubbles in samples implanted to critical dose. The distributions are approximately normal, and there is no significant difference in the two means when the experimental uncertainty is taken into account.

The other important consideration is the bubble spacing, which for the random arrays was deduced from Debye–Scherrer rings in diffraction mode. The average bubble spacing deduced from the diameter of these rings matched the $\{110\}_b$ spacing for the ordered bubbles.

For the ordered arrays, the lattice constant was remarkably consistent across the range of temperatures, being typically 5 nm. The dense-packed planes are then spaced at 3.6 nm, which is consistent with the bubble spacing found for randomly arrayed bubbles of a similar size.

4. Discussion

The results in Section 3 demonstrate the existence of a temperature threshold for molybdenum in the range 390–470 K, but with samples at each temperature being implanted to different doses, it is important to establish that a similar level of bubble development is being attained at each temperature. The normalising factor for bubble development is the dose level where radiation blistering is first detected.

4.1. Model of bubble evolution with dose

At the implantation temperatures investigated here, radiation blistering of the implanted surface is a universal phenomenon at high helium doses. Although the microstructural changes leading to blister formation are recognised to be complicated, the available evidence is consistent with the following model for helium-induced blistering near $0.2T_m$. In the early stages of implantation,

helium precipitates out to form bubbles, which are random but uniform in size (up to approximately 1.5 nm in diameter). As the implantation progresses, patches of order develop in the bubble array. These patches grow until eventually the fully developed gas–bubble superlattice is formed. For local helium concentrations just beyond the superlattice stage, the bubble arrays remain ordered as they coarsen through bubble coalescence [15]. Typical bubble diameters in these coarser ordered structures are 4 to 6 nm. As the concentration of helium in the surrounding matrix increases further, bubble diameters increase monotonically. The bubbles are largest at depths where the helium concentration is greatest, i.e. at depths near the mean projected range R_p. For bubble diameters larger than about 6 nm the arrays are no longer ordered but cavity sizes are approximately uniform. It can be speculated that radiation blistering finally results from inter-bubble fracture between very large (> 20 nm diameter) random bubbles at depths around R_p. At depths away from R_p, the bubble structures are much less advanced. For example, in near-surface specimens taken from targets implanted to ϕ_c at temperatures $\approx 0.2T_m$, the bubbles are still at or just beyond the superlattice stage. This interpretation suggests that samples implanted at different temperatures may be assumed to be at a similar stage of bubble evolution for a given depth when the onset of radiation blistering is detected on the sample surface. It is interesting to examine some of the results obtained here at several different temperatures in the context of this model of bubble evolution developed for temperatures $\approx 0.2T_m$.

4.1.1. Superlattice development with dose at $0.2T_m$

For targets implanted near a temperature of $0.2T_m$, the differences in the ordered structures in near-surface specimens between the two dose levels $0.75\phi_c$ and ϕ_c, are consistent with the above model for development of the ordered bubble structure within the superlattice stage. For a dose of $0.75\phi_c$ the bubble ordering has a three-dimensional character but is within domains. The bubbles in any given domain have a similar diameter and similar inter-bubble spacing. However, over the many domains contributing to the SADPs the average bubble diameter and spacing varies widely. The bubble structure evolves until, by a dose of ϕ_c the superlattice is much more homogeneous, with a much higher degree of uniformity of bubble diameter and spacing.

4.1.2. Variation of ϕ_c with T

The constant dose experiment outlined in Section 3.4 suggests that at low temperatures, higher doses would be required to produce the same level of bubble development. The critical dose for radiation blistering increases with decreasing temperature. These two observations suggest that radiation blistering may be associated with a particular stage of bubble development as proposed in the model of Section 4.1. This is confirmed by near-surface specimens taken from targets implanted to ϕ_c at different temperatures. These specimens showed almost identical bubble structures in terms of the size and spacing of bubbles, differing only in respect of the degree of bubble ordering (see Section 3.5). These results justify normalising the helium dose at each different temperature to ϕ_c so as to obtain comparisons for similar stages of bubble development.

4.2. Degree of ordering

In a bcc lattice, the dense-packed planes are the {110}, and these are the lowest order reflections observed from a bcc lattice (depending on the zone axis), the 100 type reflections being crystallographically disallowed. In general, only the lowest order reflections are observed from the bubble lattice, possibly due to its comparatively short-range order. In addition, the intensity profile for diffraction from bubbles strongly favours diffraction at small angles and drops off sharply as the angle increases [18].

The presence of reflections from the {110} planes in the bubble lattice does not necessarily mean that the bubbles are ordered in three dimensions; they may simply be ordered onto the {110} planes and not within them. The diffraction pattern may then arise from a superposition of reflections from each set of {110} planes [12]. Some evidence of the dense-packed planes intersecting to form a true, three-dimensional lattice is required. Good evidence is provided by the appearance of disallowed reflections from the low index {100} planes. Disallowed reflections arise from imperfections in the bubble lattice, which allow some relaxation of the crystallographic selection rules. Also, the relatively short-range order of the bubble lattice means that rules formulated with the assumption of an infinite lattice no longer strictly apply.

In ordered bubble arrays found in samples implanted at 570 K, several examples of disallowed reflections were found, indicating a well-developed three-dimensional bubble lattice. There were also examples of disallowed reflections at the lower temperatures where ordering was observed.

In cases where the bubble array was random, rings or discs commonly appeared in the SADP with a radius comparable to the radial separation of 110_b spots in the case of ordered bubbles. A distinct ring indicates a strongly preferred inter-bubble separation but no preferred direction, whereas a disc implies a range of inter-bubble separations and no preferred direction. Where there is a ring, indicating a preferred bubble spacing, the bubbles may be at an early stage in the ordering process.

In early work in molybdenum [2], during the implantation of a specimen in situ in an electron microscope, a Debye–Scherrer ring was observed prior to the appearance of satellite reflections in the diffraction pattern. This observation is consistent with a dose threshold for bubble ordering. A dose threshold for the related phenomenon of void ordering has been established by Liou et al. [19].

4.3. Vacancy motion

The experimental evidence clearly demonstrates the existence of a lower temperature threshold for bubble ordering. What then, is the temperature influencing? To our knowledge none of the models of bubble ordering has predicted the existence of such a threshold. A leading model is based on the two-dimensional diffusion of host interstitials through the crystal lattice, see for example, Ref. [20]. Interstitials, however, are very mobile even at low temperatures and so there seems no ready explanation for a lower temperature threshold to bubble ordering simply in terms of the onset of interstitial motion.

The mobilisation energy of a vacancy is approximately ten times that of an interstitial. This leads us to suggest that some degree of thermally induced vacancy motion is a prerequisite for bubble ordering. Here we suggest that the capture of vacancies by bubbles may be a necessary condition for the growth, movement and subsequent ordering of bubbles. A simple order of magnitude calculation supports this suggestion.

The jump frequency for a vacancy (the average frequency at which a vacancy moves between atomic sites) can be expressed

$$\nu = \nu_0 \exp\left[\frac{-E_{mv}}{kT}\right],$$

where E_{mv} is the migration energy for vacancies. Data from Ref. [21] give ν_0 as 1.3×10^{13} s^{-1} and E_{mv} as 1.35 eV for molybdenum. The bubble superlattice parameter found here for molybdenum is $\simeq 5$ nm. For a bcc lattice this corresponds to a nearest-neighbour bubble distance of $\simeq 4$ nm. Each bubble can be thought of as capturing vacancies from a spherical volume of radius $\simeq 2$ nm (half the nearest-neighbour distance) centred on the bubble. The root mean square displacement, R_{rms}, for the thermally induced random walk of vacancies at temperature T (K) is given by

$$R_{rms} = (\nu t)^{0.5} l,$$

where l is the vacancy jump length in molybdenum ($= 0.27$ nm), and t is the time interval considered. Here vacancies are being generated throughout the implantation process. To allow for this we take t to be half the implantation time, i.e. $t = 1.5 \times 10^4$ s. Setting R_{rms} equal to 2 nm and solving for T gives the result $T = 440$ K, a figure that correlates well with the observed threshold temperature (in the range between 390 K and 470 K). Although the level of agreement found here can be regarded as somewhat fortuitous given the assumptions made it seems clear that the vacancy jump frequency becomes significant (i.e. the effective migration range becomes comparable with the inter-bubble separation), at temperatures in the region of the observed threshold temperature.

It is clear that any model of bubble development will need to include vacancy mobility as a parameter if a complete description is to be obtained for molybdenum.

5. Conclusion

It is concluded that there is a lower temperature threshold for bubble ordering in molybdenum in the temperature range $0.14T_m$ to $0.16T_m$ (390–470 K) for a helium dose rate of $\approx 10^{18}$ He^+ m^{-2}. At temperatures just above the threshold (0.16 to $0.20T_m$), bubble superlattices were formed with lattice constants similar to those found in earlier research for temperatures of $0.20T_m$ and above.

At temperatures below the threshold, $0.14T_m$, bubble arrays can be formed which have bubbles of the same diameter and average spacing as the ordered arrays above the threshold. Without exception the arrays formed below the threshold are random. The calculated helium and damage levels for these random arrays are typically well above those calculated for the ordered arrays formed above the threshold. The results of ion-beam milling, and of implanting above the threshold at doses less than ϕ_c, suggest that below the temperature threshold not even a high dose level will produce ordering, but above the threshold, the dose level affects the degree of ordering. Above the temperature threshold, bubble ordering occurs initially in domains. Within any given domain the bubbles are of similar size and spacing. However, from one domain to the next there are variations in size and spacing. With increasing helium dose this domain structure decreases by evolving towards a homogeneous superlattice with a high degree of uniformity of bubble size and spacing.

The temperature range $0.14T_m$ to $0.16T_m$ corresponds to temperatures where the effective migration rate of vacancies (in terms of the root mean square displacement for thermal random walk over the duration of implantation) becomes comparable with the separation of nearest-neighbour bubbles in the gas–bubble superlattice. This strongly suggests that in molybdenum vacancy mobility plays an important role in the development of ordered bubble structures.

Acknowledgements

We thank K.L. Reader, R.W. Thomson B.J. Martin, Y. Morrison and T.T. Young of Victoria University of Wellington for technical assistance. We thank Dr P.W. Gilberd of Victoria University of Wellington, Drs D.J. Mazey and J.H. Evans formerly of AEA Reactor Services, Harwell Laboratory, UK, and Professor A. Seeger of the Max-Plank-Institut für Metallforschung, Institut für Physik, Stuttgart for stimulating discussions relating to this work.

References

[1] S.L. Sass, B.L. Eyre, Philos. Mag. 27 (1973) 1447.
[2] D.J. Mazey, B.L. Eyre, J.H. Evans, S.K. Erents, G.M. McCracken, J. Nucl. Mater. 64 (1977) 145.
[3] P.B. Johnson, D.J. Mazey, Nature 276 (1978) 595.
[4] P.B. Johnson, D.J. Mazey, Nature 281 (1979) 359.
[5] P.B. Johnson, D.J. Mazey, J. Nucl. Mater. 93&94 (1980) 712.
[6] W. Jäger, J. Roth, J. Nucl. Mater. 93&94 (1980) 756.
[7] D.J. Mazey, J.H. Evans, J. Nucl. Mater. 138 (1986) 16.
[8] J.H. Evans, A.J.E. Foreman, R.J. McElroy, J. Nucl. Mater. 168 (1989) 340.
[9] D.R.G. Mitchell, S.E. Donnelly, Radiat. Eff. 14 (1990) 253.
[10] K. Krishan, Radiat. Eff. 66 (1982) 121.
[11] J.H. Evans, in: D. Walgraef, N.M. Ghoniem (Eds.), Proc. NATO Advanced Study Institute on Patterns, Defects and Instabilities, Cargese, Corsica, 1989, Kluwer Academic, Dordrecht, 1990.
[12] P.B. Johnson, in: J.S. Evans and S.E. Donnelly, Fundamental Aspects of Inert Gases in Solids, Plenum, New York, p. 167.
[13] P.B. Johnson, D.J. Mazey, J. Nucl. Mater. 218 (1995) 273.
[14] P.B. Johnson, K.L. Reader, R.W. Thomson, J. Nucl. Mater. 231 (1996) 92.
[15] P.B. Johnson, P.W. Gilberd, Nucl. Instr. and Meth. B 127& 128 (1997) 734.
[16] J.F. Ziegler, J.P. Biersack, U. Littmark, The Stopping and Range of Ions in Matter, Pergamon, New York, 1985.
[17] P.B. Johnson, D.J. Mazey, J. Nucl. Mater. 111&112 (1982) 681.
[18] K.J. Stevens, Ph D thesis, Victoria University of Wellington, 1993.
[19] K.Y. Liou, H.V. Smith, P. Wilkes, G.L. Kulcinski, J. Nucl. Mater. 83 (1979) 335.
[20] J.H. Evans, J. Nucl. Mater. 132 (1985) 147.
[21] I.A. Schwirtlich, H. Schulz, Philos. Mag. A 45 (5) (1980) 600.